

## Validation of a Thermodynamic Retrieval Technique by Application to a Simulated Squall Line with Trailing Stratiform Precipitation

J. SUN\* AND R. A. HOUZE, JR.

*Department of Atmospheric Sciences, University of Washington, Seattle, Washington*

(Manuscript received 30 November 1990, in final form 11 September 1991)

### ABSTRACT

A thermodynamic retrieval technique, which uses the equation of motion in conjunction with the thermodynamic equation, is validated in a two-dimensional numerical model simulation of a squall line with a trailing stratiform region. Model wind and reflectivity output are used as input to the retrieval. The availability of model thermodynamic output allows us to examine the performance of the retrieval. The computational technique involved is found to be valid. When the retrieval is applied to the time-averaged model wind fields, reasonably accurate results are obtained for the stratiform region, but errors arise for the convective region because of the neglect of eddy correlations of the temporally fluctuating wind components. Application of the retrieval to instantaneous model wind fields demonstrates that very high time resolution is needed in the wind data (< about 2 min) to obtain reliable results where time changes are large and nonlinear.

### 1. Introduction

Doppler radar observational technology provides the opportunity to study convective cloud systems by indicating the detailed air circulation inside of them. In addition, it is possible to retrieve thermodynamic parameters from the indicated wind field. Gal-Chen (1978) and Hane and Scott (1978) initiated thermodynamic retrieval work by proposing an analysis based on the equation of motion, the radar-observed spatial fields of the wind components, and their temporal tendency to determine the temperature and pressure perturbations. However, the retrieval was possible only on individual horizontal planes, and the solution was dependent on an undetermined constant for each horizontal plane. Thus, only the deviations of temperature or pressure with respect to their horizontal averages could be determined. Roux (1985, 1988) attempted to resolve this problem by using the equation of motion in conjunction with the thermodynamic equation. Further improvement of the retrieval is described in Roux and Sun (1990, henceforth referred to as RS). Although their application of this technique to a West African squall line observed during the COPT 81 (Convection Profonde Tropicale 1981) experiment produced physically reasonable results, a strict vali-

ation of the retrieval technique was not conducted. The main objective of this paper is to carry out the validation by means of using the output of a two-dimensional numerical cloud model as input to the retrieval.

Validation of the earlier retrieval technique was carried out by Hane et al. (1981). They used the output from the three-dimensional model of Klemp and Wilhelmson (1978) in place of observed data to test their method for retrieving temperature and pressure deviations from the horizontal means. Their rather complete set of sensitivity tests included the evaluations of local time derivatives, turbulence, cloud-water content, rainwater content, errors in the velocities, and filter technique. Klemp and Wilhelmson's model produced a single storm initiated by a thermal perturbation, which grew and split into left- and right-moving storms after 30 min. The right mover grew and, after 80 min, decreased gradually. The retrieval of Hane et al. (1981) was fixed around 90 min. Their results showed that the local time derivatives estimated from a 30-s time span gave virtually the same temperature-deviation structure as the original one of the numerical model; even the 4-min span estimation resulted in an excellent agreement. When the local derivative was eliminated, the solution was judged to be useful in its general pattern despite a deterioration of details. This reflected the fact that the retrieval was done at a moment (90 min after the initiation) when the storm evolution was linear and relatively small. The results also showed that it is important to adequately filter the retrieved temperature deviation to reduce the errors produced by the noise associated with the velocity fields.

\* Present affiliation: Atmospheric Environment Service, Environment Canada, Downsview, Ontario, Canada.

Corresponding author address: Dr. Ju Sun, Universite du Quebec a Montreal, Departement de Physique, Montreal H3C 3P8 Quebec, Canada.

The test of Hane et al. (1981) was for the earlier retrieval technique in which only the equation of motion was used. In addition, their study was concerned with the Klemp–Wilhelmson (1978) simulation of a supercell thunderstorm. In this type of storm, the convective updrafts are especially strong, broad, and slowly varying. These characteristics make the storm more amenable to retrieval analysis since the basic radar signals are so strong and definite. The supercell, however important, is relatively rare.

Therefore, besides working with a more complete type of retrieval, we focus on a different type of storm: the squall line with a trailing stratiform region. This type of convective system, studied by many investigators (e.g., Smull and Houze 1985, 1987; RS), offers more challenges to retrieval and is important because so many mesoscale convective systems exhibit its basic properties (Houze et al. 1990). Its convective cells are of the more short-lived and smaller-scale variety seen in common thunderstorms [such as those seen in the Thunderstorm Project (Byers and Braham 1949)]. In addition to the convective cells, it has a mesoscale area of stratiform cloud and precipitation whose air motions are 2–3 orders of magnitude weaker than those of the convective cells but at the same time covering a broader area and varying slowly in time. Thus, both the convective and stratiform portions of the squall line with a trailing stratiform region present new challenges to the retrieval. The convective cells have a highly fluctuating pattern, which is difficult to capture exactly in radar data. The effects on the retrieval of these fluctuations in space and time need careful evaluation. The broad scale of a convective system with stratiform precipitation makes it necessary in some research to construct a composite of radar data collected at several times and locations to obtain a more complete picture of the storm (e.g., Biggerstaff and Houze 1991a,b). Considerable filtering of the data is necessary to smooth out the composite patterns to see the weak but widespread vertical air motions in the stratiform region. It is important to know whether the retrieval technique can be applied to such filtered and smoothed fields.

In this paper we investigate the reliability of applying the thermodynamic retrieval technique of RS to a squall line with a trailing stratiform region. We will carry out tests of the retrieval on the output of a successful model simulation of such a squall-line system. As was the strategy of Hane et al. (1981), we will apply the retrieval to the model-generated wind and precipitation fields (i.e., the fields that would be observed by radar) and attempt thereby to reproduce the model-calculated thermodynamic fields. In particular, we will use the model output of Fovell and Ogura (1988), who used a two-dimensional nonhydrostatic model to replicate the behavior of the 22 May 1976 squall-line system studied by Ogura and Liou (1980) and Smull and Houze (1985, 1987). That storm is reasonably repre-

sentative of the class of storms characterized by a squall line with a trailing stratiform region. We focus on three specific objectives: (i) the computational technique of the retrieval is tested; (ii) the ability of the retrieval to diagnose time-mean fields from the model is tested as a way of indicating the applicability of the retrieval to a broad-scale radar composite of the storm; and (iii) the time resolution required in the wind and precipitation fields in order to reproduce the instantaneous storm structure is determined. The latter two tests provide an indication of the ability of the retrieval to represent accurately the thermodynamics of both the convective and stratiform regions of this common and important type of convective cloud system.

## 2. Brief review of retrieval technique

The basic premise of the retrieval is that unknown thermodynamic parameters like temperature and pressure can be deduced from observed wind velocities. These variables are related to each other through the anelastic form of the basic governing equations of the atmosphere (as given, for example, by Wilhelmson and Ogura 1972). These include the equation of motion

$$\frac{\partial \mathbf{v}}{\partial t} + (\mathbf{v} \cdot \nabla) \mathbf{v} = -C_p \theta_{v0} \nabla \pi_1 + g \left( \frac{\theta_{c1}}{\theta_0} - q_r \right) \mathbf{k} + \mathbf{F}_{\text{tur}}, \quad (1)$$

and the thermodynamic equation

$$\frac{\partial}{\partial t} (\theta_0 + \theta_1) + (\mathbf{v} \cdot \nabla) (\theta_0 + \theta_1) = S_\theta, \quad (2)$$

where  $\mathbf{v}$  is the air velocity vector,  $\theta$  is the potential temperature,  $\theta_v$  is the virtual potential temperature,  $\pi$  is the nondimensional pressure perturbation [ $\pi = (p/1000 \text{ mb})^{R/C_p}$ ,  $\pi_1 = p_1 (C_p \theta_{v0} \rho_0)^{-1}$ ],  $R$  is the gas constant for dry air, and  $C_p$  is the specific heat at constant pressure for dry air. The subscale turbulence force is  $\mathbf{F}_{\text{tur}}$ , with  $F_{\text{tu}}$  and  $F_{\text{tw}}$  as  $x$  and  $z$  components. The subscript 0 indicates the environment base state, and 1 indicates the perturbation with respect to the base state. The parameter  $\theta_{c1}$  is referred to by Roux et al. (1984) as the virtual cloud potential temperature perturbation [ $\theta_{c1} = \theta_1 + (0.61q_{v1} - q_c)\theta_0$ ];  $q_{v1}$  is the water vapor content perturbation;  $q_c$  is the cloud-water content;  $q_r$  is the precipitation content, which can be estimated from the radar reflectivity through theoretical or empirical formulation ( $q_r$  in this test is calculated from model reflectivity output); and  $S_\theta$  is the heat source or sink.

Since we are interested in two-dimensional structure, (1) and (2) are rearranged to obtain

$$A_x = \frac{\partial \pi_1}{\partial x} = - \frac{1}{C_p \theta_{v0}} \left[ \frac{\partial u}{\partial t} + (\mathbf{v} \cdot \nabla) u - F_{\text{tu}} \right] \quad (3)$$

$$A_z = \frac{\partial \pi_1}{\partial z} = -\frac{1}{C_p \theta_{v0}} \times \left[ \frac{\partial w}{\partial t} + (\mathbf{v} \cdot \nabla) w - F_{tw} - g \left( \frac{\theta_{c1}}{\theta_0} - q_r \right) \right] \quad (4)$$

$$B_x = \frac{\partial \theta_{c1}}{\partial x} = \frac{\theta_0}{g} \left\{ \frac{\partial}{\partial x} \left[ \frac{\partial w}{\partial t} + (\mathbf{v} \cdot \nabla) w + g q_r - F_{tw} \right] - \theta_{v0} \frac{\partial}{\partial z} \left[ \frac{1}{\theta_{v0}} \left( \frac{\partial u}{\partial t} + (\mathbf{v} \cdot \nabla) u - F_{tu} \right) \right] \right\} \quad (5)$$

$$B_t = u \frac{\partial \theta_{c1}}{\partial x} + w \frac{\partial \theta_{c1}}{\partial z} = -\frac{\partial \theta_1}{\partial t} - w \frac{d\theta_0}{dz} - 0.61 \theta_0 w \frac{dq_{v0}}{dz} + \delta_s \left[ -\frac{L}{C_p \pi_0} w \gamma_{sa} + 1.61 \theta_0 w \frac{dq_{sa}}{dz} + \theta_0 F(q_r) \right] + (1 - \delta_s) \left[ \frac{L}{C_p \pi_0} F(q_r) - 0.61 \theta_0 F(q_r) \right]. \quad (6)$$

Details of the derivation of (3)–(6) are given by RS. Equation (5) provides information about the horizontal gradient of  $\theta_{c1}$  based on the equation of motion and deduced from air motions and their evolution. Equation (6) combines information on the horizontal and vertical gradients of  $\theta_{c1}$  based on the thermodynamic equation for saturated ( $\delta_s = 1$ ) and nonsaturated ( $\delta_s = 0$ ) regions, respectively. The distinction between the saturated and nonsaturated regions is made with a function defined as  $F(q_r) = \partial q_r / \partial t + (\mathbf{v} \cdot \nabla) q_r + \partial / \partial z (\rho_0 v_t q_r)$ . When it is positive, cloud water is being transformed to precipitation water so that the air is saturated and, conversely, it represents the evaporation rate associated with rainwater in a nonsaturated region. In the saturated region, the air parcels follow moist-adiabatic motion, therefore, the latent heat release is approximately obtained from the moist-adiabatic lapse rate  $\gamma_{sa}$ . Once  $A_x$ ,  $A_z$ ,  $B_x$ , and  $B_t$  are known, we can find the  $\theta_{c1}$  and  $\pi_1$  fields that fit in the least-squares sense by minimizing the functions  $F_\theta$  and  $F_\pi$  defined as

$$F_\theta = \iint \left[ \left( \frac{\partial \theta_{c1}}{\partial x} - B_x \right)^2 + \left( \frac{u}{V} \frac{\partial \theta_{c1}}{\partial x} + \frac{w}{V} \frac{\partial \theta_{c1}}{\partial z} - B_t \right)^2 \right] dx dz, \quad (7a)$$

$$F_\pi = \iint \left[ \left( \frac{\partial \pi_1}{\partial x} - A_x \right)^2 + \left( \frac{\partial \pi_1}{\partial z} - A_z \right)^2 \right] dx dz, \quad (7b)$$

where  $V = (u^2 + w^2)^{1/2}$ , and the integrations are carried out over the whole domain.

When the right-hand side of (5) is estimated from real Doppler radar data, it is often difficult or impossible to estimate the local derivatives  $\partial u / \partial t$  and  $\partial w / \partial t$ , and it may be necessary in practice to avoid these terms by seeking relatively steady-state features in the data or by applying the technique to mean or composite wind fields. If the latter is done (e.g., Sun and Roux 1988; RS), however, an error is introduced because the average of the terms  $(\mathbf{v} \cdot \nabla) w$  and  $(\mathbf{v} \cdot \nabla) u$  are estimated from the mean velocity fields as  $(\bar{\mathbf{v}} \cdot \nabla) \bar{w}$  and  $(\bar{\mathbf{v}} \cdot \nabla) \bar{u}$ , where the overbars represent time averages. This estimate ignores the contributions of eddy fluxes  $(\mathbf{v}' \cdot \nabla) w'$  and  $(\mathbf{v}' \cdot \nabla) u'$ , where the prime represents a deviation from the time average. These fluxes may be significant in regions of convection, where time scales of changes are short compared to the length of the averaging period. One of the main objectives of this paper is to evaluate how much impact the neglect of the eddy flux term has on the retrieval of thermodynamic fields of the squall line with a trailing stratiform region. This determination can be made with the model results used as input. The simulated squall line became rather steady after about 350 min into the simulation for averaging times far longer than the time scale of a convective cell ( $\sim 30$  min). Mean model fields were averaged for the simulation time period 540–670 min, which encompassed four convective-cell life cycles. In these average fields,  $\partial u / \partial t = \partial w / \partial t = 0$ , and the error in the retrieval is entirely associated with the eddy fluctuation terms. This error can be found since the mean thermodynamic field retrieved from the model mean winds and reflectivity can be compared to the actual model-calculated mean thermodynamic fields, which contain the effects of the fluctuating winds, as well as the mean winds. This comparison will be discussed in subsequent sections.

The error determined in this way should be viewed cautiously as a minimum error. In applying the retrieval to a real case in which the radar data have been used to form a composite analysis, additional errors will be associated with the fact that  $\partial u / \partial t$  and  $\partial w / \partial t$  may not be truly zero, as well as the fact that the eddy correlations are not accounted for.

### 3. Description of model output

Fovell and Ogura's (1988) simulation was carried out with an anelastic two-dimensional model similar to that of Soong and Ogura (1980), in which the Coriolis force is neglected and the turbulence term is set to a very small value. The horizontal grid space is 1 km and the vertical grid space is stretched from 200 m just above the ground to 700 m near the 12-km level. The simulation was initiated with the environment represented by the sounding data shown in Fig.

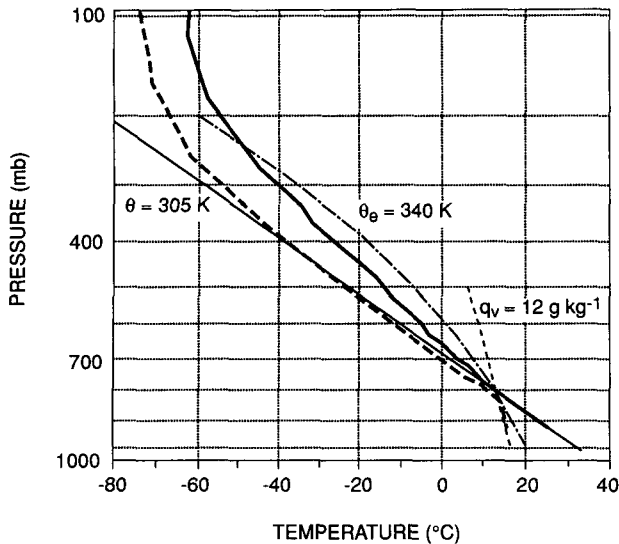


FIG. 1. Sounding data serve to initiate the model simulation and as the undisturbed base state in the retrieval (adapted from Fovell and Ogura 1988).

1. The same data serve as the undisturbed base state in the retrieval discussed below. The time step used in these calculations was 5 s. It produced a moving squall line with periodic formation of convective cells at its leading edge. In the “no-hail” case, which was the most realistic, the propagation speed reached  $16 \text{ m s}^{-1}$ . The multicellular structure appeared in both the time history of the domain maximum vertical velocity (Fig. 2a) and the surface rainfall pattern (Fig. 2b). The individual cells moved rearward, and each complete cycle lasted 32 min. The time-averaged fields over several complete cycles exhibit the primary mean characteristics of observed squall lines (Fig. 3). The system-relative horizontal airflow is front to rear at the leading edge and above the 3-km level behind, with an axis of maximum at the 6-km level. Below the front-to-rear flow, a rear inflow enters the system between the 1- and 3-km levels. The rear-to-front flow traverses the whole region and reaches the front edge where it encounters the unstable air of the prestorm environment. The strongest vertical motions ( $11 \text{ m s}^{-1}$ ) are found in the leading portion of the storm, where the intense convective cells were located. A deep downdraft originating at upper levels is located just behind the region of upward motion. Just to the rear of this feature is a wider and less intense updraft at levels above 6 km. This feature and the broad downdraft below the wide updraft coincide with the front-to-rear flow seen Fig. 3b. The potential temperature perturbations  $\theta_1$  are positive at upper levels, and the axis of maximum  $\theta_1$  coincides with that of the front-to-rear flow. The negative perturbations at lower levels coincide with the rear-to-front flow and form the cold pool, which ex-

hibits a bulging head at its leading edge. This structure is typical of thunderstorm cold pools, which consist of negatively buoyant downdraft air. As downdrafts encounter the ground, they propagate forward with the head at the leading edge (see Charba 1974; Wakimoto 1982; Droegemeier and Wilhelmson 1987 for details). The more buoyant environmental air meeting the cold-pool head is forced up over the head at the gust front, which is the warm edge of the cold pool, where the sharp convergence is concentrated. A narrow zone of warm air is seen to extend upward and rearward from the gust front in Fig. 3d.

Thus far, we see that the time-averaged fields possess many typical features of observed squall lines in both the convective and trailing stratiform region (Houze et al. 1989). Since the capability to collect data is limited, especially when the storm has a mesoscale structure that is much larger than any individual Doppler radar range and one radar scan covers only a part of the storm, the assumption of steady state is sometimes necessary to make a composite analysis so that the overall structure of a storm can be deduced (e.g., Sun and Roux 1988; RS). The time-averaged fields of model output represent a pseudosteady state, which is actually an indication of the repetitiveness of the time-dependent fields, but can be usefully compared to a composite analysis of a squall line. How well the thermodynamic retrieval technique diagnoses the thermodynamic fields from the model time-averaged wind fields can be tested. If this test is successful the technique can be applied with more confidence to a composite data analysis of a squall line.

#### 4. Retrieval based on the time-averaged model wind fields

Unlike the work of Hane et al. (1981), the equation sets are not used in exactly the same form as the model simulation, nor for the same grid mesh. Instead of a stretched grid in the vertical as used in the simulation, a uniform grid mesh in both horizontal and vertical directions is adopted. The grid space is 1 km in the horizontal and 500 m in the vertical. The first objective of this study listed in the Introduction may be restated as the question: Can we find the  $\theta_{c1}$  field without any purely computational flaw if the terms  $B_x$  and  $B_t$  are deduced correctly? The second objective may be rephrased as: Is it possible to estimate the terms  $B_x$  and  $B_t$  correctly from the steady time-mean winds? The first question is now addressed to make sure that there is no distortion associated with the computational technique before an attempt is made to answer the question of objective (ii).

##### a. Validation of the computational step

The most important advance of this retrieval analysis over that of Gal-Chen (1978) or Hane and Scott (1978)

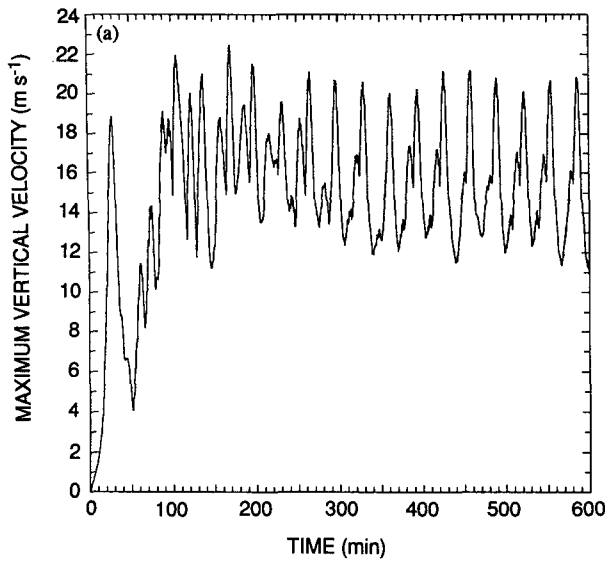
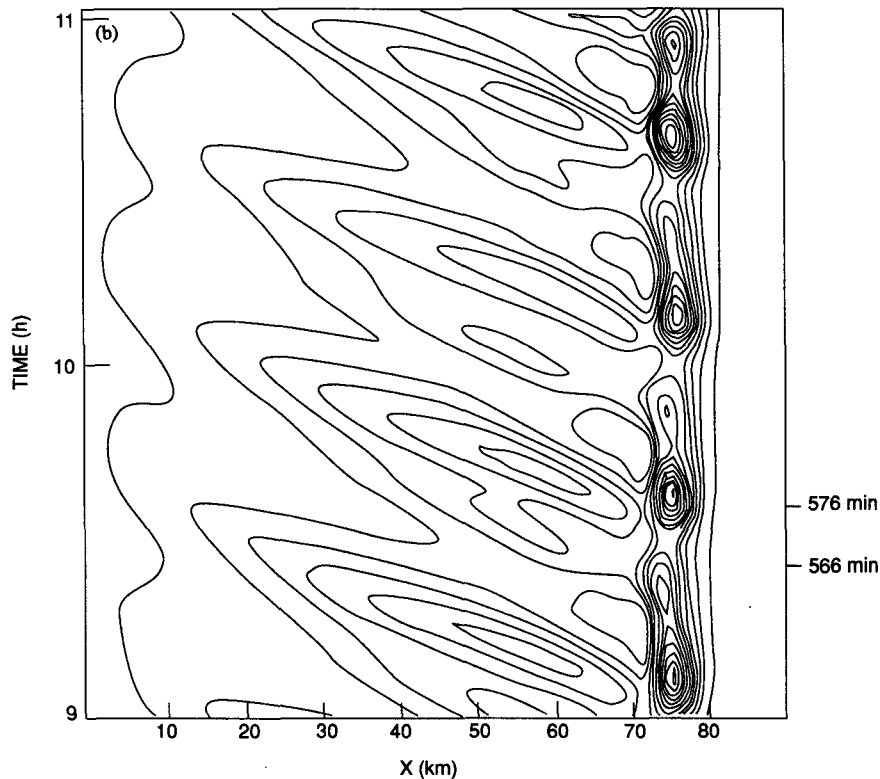


FIG. 2. (a) Time history of the domain maximum vertical velocity ( $\text{m s}^{-1}$ ) for the no-hail run; (b) system-relative surface rainfall intensity for the no-hail run between 9 and 11 h (contour interval is  $6 \text{ mm h}^{-1}$  starting from  $1 \text{ mm h}^{-1}$ ). The abscissa is the horizontal section of model domain (km), the ordinate is the time of simulation (h) (provided by R. Fovell).



is the capability to obtain the pressure and temperature perturbations in vertical planes as well as in the horizontal. This difference is clearly demonstrated in (7a), which includes the vertical gradient of  $\theta_{c1}$  in addition to the horizontal gradients. Unfortunately, in the second term of (7a), the vertical gradient of  $\theta_{c1}$  is combined with the vertical velocity. Similarly, the horizontal gradient of  $\theta_{c1}$  is combined with the horizontal

velocity. In areas of small velocities, the solution of (7a) becomes unstable. In the stratiform region of the squall line, the vertical motions are often very weak. The typical value is  $\sim 10^{-1} \text{ m s}^{-1}$ . To avoid computational instability, a weighting function is assigned to the second term of (7a) in order to decrease its contribution in the retrieval when the speed is under a specific threshold. Thus, (7) is rewritten as

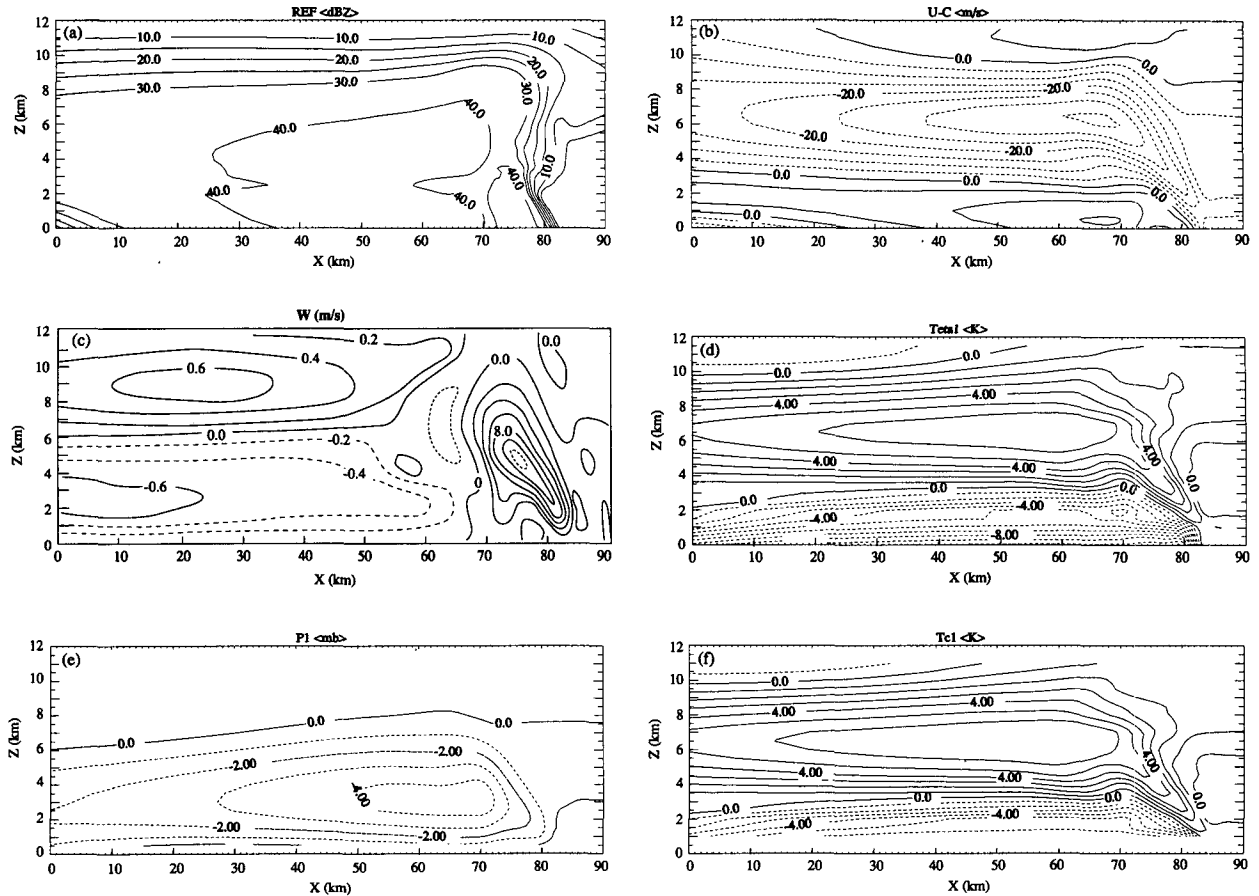


FIG. 3. Time-averaged model fields. (a) Radar reflectivity (contour interval 5 dBZ); (b) system-relative horizontal velocity ( $5 \text{ m s}^{-1}$ ); (c) vertical velocity ( $2 \text{ m s}^{-1}$ ; contours with interval of  $0.2 \text{ m s}^{-1}$  are added in the stratiform region ( $X < 60 \text{ km}$ ) to show more details); (d) potential temperature deviation from base state (1 K); (e) pressure perturbation (1 mb); (f) virtual cloud potential temperature perturbation (1 K).

$$F_{\theta} = \iint \left[ \left( \frac{\partial \theta_{c1}}{\partial x} - B_x \right)^2 + \mu_0 f(V) \left( \frac{u}{V} \frac{\partial \theta_{c1}}{\partial x} + \frac{w}{V} \frac{\partial \theta_{c1}}{\partial z} - B_t \right)^2 + \mu_1 h(V, w) \left( \frac{\partial \theta_{c1}}{\partial z} \right)^2 \right] dx dz, \quad (8a)$$

$$F_{\pi} = \iint \left[ \left( \frac{\partial \pi_1}{\partial x} - A_x \right)^2 + \nu_0 \left( \frac{\partial \pi_1}{\partial z} - A_z \right)^2 \right] dx dz, \quad (8b)$$

where  $f(V) = V^4(V^4 + V_0^4)^{-1}$ ,  $h(V, w) = 1 - f(V)f(w)$  and  $\mu_0$ ,  $\mu_1$ , and  $\nu_0$  are constants. The third term in (8a) means that the vertical gradients of  $\theta_{c1}$  should be small if the vertical motions are weak (see RS for details).

Although the improved retrieval technique represented by (8) has been applied to a real case of a West

African squall line with a broad trailing stratiform region with seemingly reasonable results (see RS), the technique has not yet been validated rigorously. The availability of Fovell and Ogura's (1988) model simulation fields provides an excellent opportunity to accomplish the task. Their simulation produced a squall line with both an intense convective and extended stratiform region. In the latter, the upward motions occupy the region above 6 km with a maximum of  $60 \text{ cm s}^{-1}$ . At lower levels, downward motions of similar magnitude are found. A zone of virtually no vertical velocity lies between them.

The present concern is whether the  $\theta_{c1}$  field can be determined correctly, given accurate values of  $B_x$  and  $B_t$ . The best way to obtain the accurate  $B_x$  and  $B_t$  is, of course, to take them directly from the model output  $\theta_{c1}$  field. The model output  $\theta_{c1}$  field was not directly provided; therefore, it was calculated from the model fields of potential temperature perturbation, cloud-water content, and water vapor perturbation, according

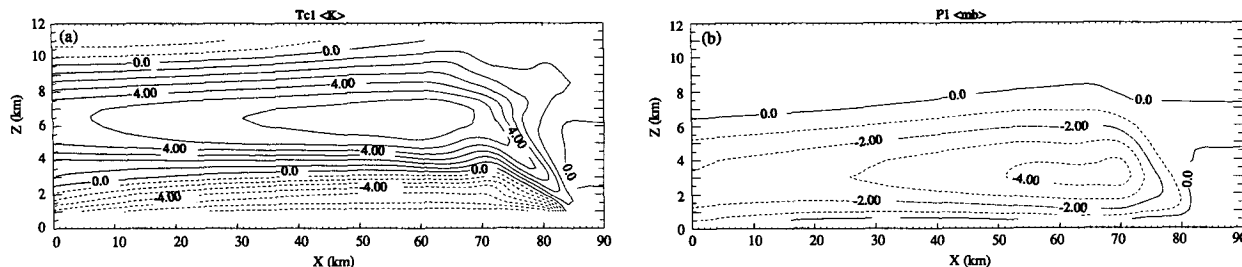


FIG. 4. (a) Virtual cloud potential temperature perturbation retrieval from  $B_{xm}$  and  $B_{tm}$  deduced from the model-output  $\theta_{c1}$  field; (b) pressure perturbation retrieved from  $A_{xm}$  and  $A_{zm}$  deduced from the model-output  $p_1$  field.

to the formula mentioned earlier. Figure 3f shows the result. The maximum differences between  $\theta_1$  and  $\theta_{c1}$  are  $\pm 0.5^\circ\text{C}$ , correlated with the maximum of water vapor perturbations of  $\sim 0.2 \text{ g kg}^{-1}$ . The effect of cloud-water content is insignificant everywhere except in the convective region, and there its contribution to  $\theta_{c1}$  is strongly offset by the water vapor perturbations. From the  $\theta_{c1}$  calculated from the model output, we compute model values of  $B_x$  and  $B_t$ , which are called  $B_{xm} = \partial\theta_{c1}/\partial x$  and  $B_{tm} = u\partial\theta_{c1}/\partial x + w\partial\theta_{c1}/\partial z$ , respectively. These are computed from the model  $\theta_{c1}$  field by finite differences. Then the procedure described by (8a) is begun, with  $B_{xm}$  and  $B_{tm}$  substituted for  $B_x$  and  $B_t$ .

To retrieve the pressure-perturbation field  $p_1$ , the horizontal gradient  $A_{xm} = \partial\pi_1/\partial x$  and the vertical gradient  $A_{zm} = \partial\pi_1/\partial z$  are derived from the simulation output  $p_1$  field<sup>1</sup> (conversion of  $p_1$  to  $\pi_1$  is given in section 2) and minimize the integral in (8b). The retrieved  $p_1$  field (Fig. 4b) is nearly identical to the simulation output (Fig. 3e). Comparison of the retrieved  $\theta_{c1}$  field (Fig. 4a) with the simulation output (Fig. 3f) is also good. From a computational point of view, there is an important difference between pressure retrieval (8b) and temperature retrieval (8a). In the case of pressure retrieval, any difference between Figs. 3e and 4b could be explained by the accuracy of the numerical algorithm, which finds the pressure field when both horizontal and vertical gradients of the pressure are known. In case of temperature retrieval, the difference between Figs. 3f and 4a may also be accounted for by the accuracy of the algorithm. However, this algorithm is different from the pressure algorithm. The temperature field is obtained from horizontal gradients of temperature and the terms  $(u\partial\theta_{c1}/\partial x + w\partial\theta_{c1}/\partial z)$ . When the vertical velocity approaches zero, the numerical solution of (8a) becomes unstable, and the temperature field becomes impossible to retrieve. That is the reason why the weighting-function constants are applied. After some trials, the best retrieved  $\theta_{c1}$  field is obtained when

the constants involved in (8a) are set in the following combination:  $V_0 = 4 \text{ m s}^{-1}$ ,  $\mu_0 = 0.2$ ,  $\mu_1 = 0$ . Despite the difficulty of introducing these weighting functions, the retrieval results in Fig. 4a show that if  $B_x$  and  $B_t$  can be estimated correctly from the observed wind field, there is virtually no obstacle to correctly retrieving the temperature perturbation  $\theta_{c1}$  field. Thus, the problem becomes how to estimate the  $B_x$  and  $B_t$  in an appropriate way. The successful temperature retrieval is especially satisfying since it indicates that the weighting functions in the retrieval were able to overcome the possible numerical instability associated with the wide regions of low vertical velocity in the time-mean fields.

#### b. Validation of the diagnostic retrieval model

The retrieval technique is based on (1) and (2). If at a specific time all terms other than temperature and pressure in these two equations were known everywhere, it is possible to determine the fields of these last two variables if only one areawide constant is given (Roux 1988). Unfortunately, the Doppler observations provide the wind and reflectivity fields only at one moment or another for a limited region. Moreover, the heat-source distribution is not obtainable from actual observational technology. It is therefore unavoidable to make certain assumptions to circumvent the restrictions of the observations.

In this study, the simulation output wind and reflectivity fields of Fovell and Ogura (1988) are used instead of real data to retrieve the temperature and pressure fields. Although available, no other additional variables from model output are used in order to evaluate the impact of assumptions on the retrieval. To simulate a composite of radar data, the case in which the model wind and reflectivity fields are time averaged over four complete cycles is considered. In this case, the local time-derivative terms in (3)–(6) vanish. The turbulence force is neglected because the parameterization of this force in Fovell and Ogura's simulation renders it to be much smaller than the advection term. The precipitation content and the fall speed are calculated from the model radar reflectivity through the relations used in RS. The assumptions concerning pa-

<sup>1</sup> The model-output  $p_1$  field is associated with an unknown areawide constant.

parameterization of heating in the thermodynamic equation have been mentioned in section 2, where (6) is deduced from (2). The moist adiabat used to approximate the latent heat release rate in saturated regions is for the wet-bulb temperature  $21^{\circ}\text{C}$ , indicated by sounding data (Fig. 1).

Figure 5 shows the retrieved temperature and pressure fields and their difference fields (i.e., retrieved minus-model fields). Except for the more irregular shapes of the contours in comparison to the simulation output (Figs. 3f,e), the overall features are evident. Positive thermal perturbations are found at upper levels with a maximum of  $5^{\circ}\text{C}$ , which is  $1^{\circ}\text{C}$  less than the model output. There are two axes of maximum: one around the 7-km level and another at 5 km. The tongue of warm air extending up from the gust front is evident in Fig. 5a, though not quite as clearly as in the model output (Fig. 3f). The negative values at lower levels indicate the cold pool formed by the evaporation of precipitation, but the cold pool is weaker (minimum of  $-5^{\circ}$  vs  $-7^{\circ}\text{C}$ ) and less extensive upward, especially in the rear of the storm. A cool-air region is also found at the highest levels toward the rear. The pressure perturbations (Fig. 5c), whose vertical structures are mainly determined by the temperature perturbations through the hydrostatic effect, show a low of  $-3$  mb at the 3.5-km level, which agrees well with the simulation (Fig. 3e). The pressure perturbation is accurate except at low levels (Fig. 5d), where the positive anomaly of the mesohigh seen in the simulation result does not quite appear at low levels, since the cold pool is not quite cool enough.

The overall structures of temperature and pressure perturbations obtained from the retrieval are thus generally representative of the simulation output. This means that the assumptions involved in the retrieval are partially justified—"partially" because some distortions do exist. For example, one warm core located at the 6.5-km level in the original  $\theta_{c1}$  field is split into two warm cores by a zone of minimum  $\theta_{c1}$  at 5.5 km. Both positive and negative perturbations are smaller than in the model storm, and the cool region is shallower and narrower (Fig. 5b).

The precipitation content deduced from the radar reflectivity is smaller than the model output precipitation field (not shown here). The maxima are  $1.6$  versus  $2.2$   $\text{g kg}^{-1}$  in the convective rain region,  $0.8$  versus  $1.1$   $\text{g kg}^{-1}$  in the stratiform rain region, and  $1.1$  versus  $5.0$   $\text{g kg}^{-1}$  in the stratiform snow region. The most substantial difference occurs in the stratiform snow region, apparently because the empirical relationship used to convert model radar reflectivity  $Z$  to precipitation content  $q_r$  in the retrieval is the same as described in RS to analyze the real case, whereas a different  $q_r$ - $Z$  relationship was used by Fovell and Ogura (1988) to convert model  $q_r$  to  $Z$ . This difference may explain the smaller rates of warming and cooling and more restricted cooling regions as being the result of less intensive condensation and evaporation. This is further indicated by temperature perturbations retrieved by using the model output precipitation  $q_r$  (Fig. 6a). Compared with Fig. 5a, stronger intensities are found in both warm and cool regions ( $6^{\circ}$  vs  $5^{\circ}\text{C}$  and  $-6^{\circ}$  vs  $-5^{\circ}\text{C}$ ). The cool region also becomes larger.

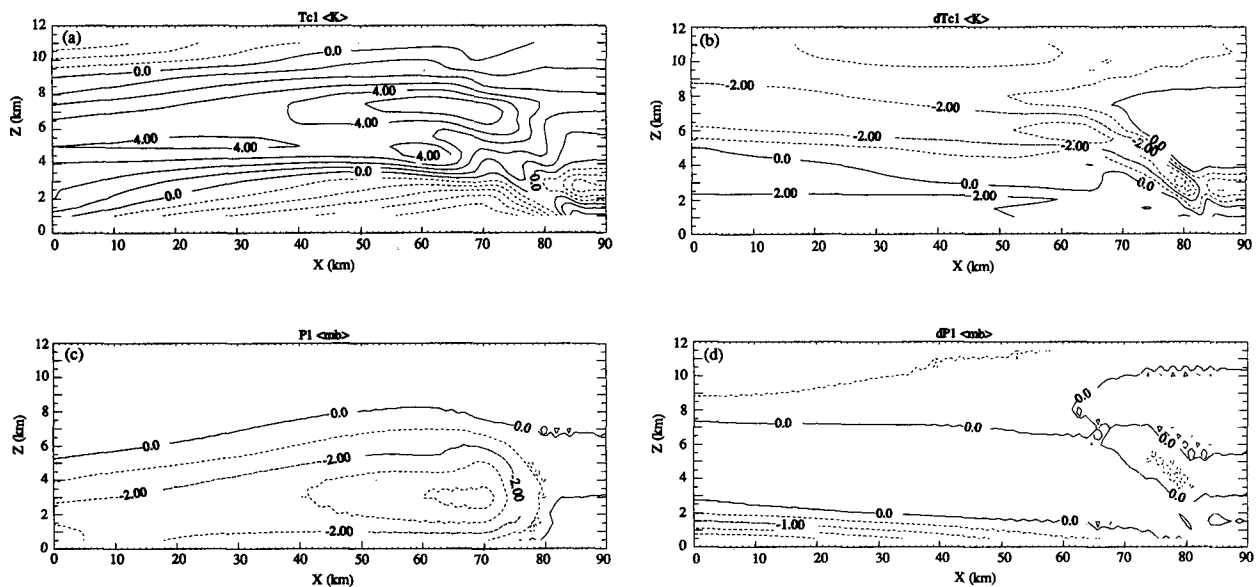


FIG. 5. (a) Retrieved  $\theta_{c1}$  field with precipitation content  $q_r$  deduced from model reflectivity by the relationship  $q_r \sim Z$  used by RS (1 K); (b)  $\theta_{c1}$  difference field (retrieved - model) (1 K); (c) retrieved  $p_1$  field (1 mb); (d)  $p_1$  difference field (retrieved - model) (0.5 mb).

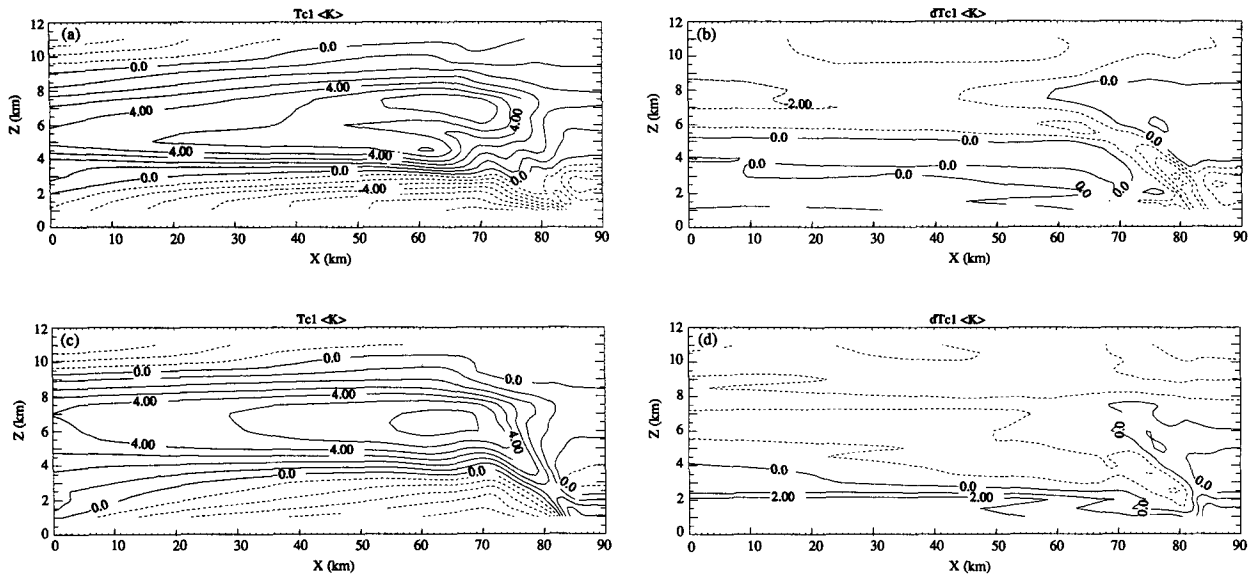


FIG. 6. (a) Retrieved  $\theta_{c1}$  field with precipitation content  $q_r$  of model output. (b) difference field of (a); (c) retrieved  $\theta_{c1}$  field from  $B_{xm}$  and  $B_r$ ; (d) difference field of (c).

The difference fields in Figs. 5b and 6b clearly show the improvement when the model-output precipitation  $q_r$  is used.

The main discrepancies in the retrieved temperature and pressure appear to be the consequence of ignoring the eddy flux terms  $(\mathbf{v}' \cdot \nabla)w'$  and  $(\mathbf{v}' \cdot \nabla)u'$  in the expression for  $B_x$  given by the right-hand side of (5). This opinion is supported by a retrieval experiment in which the  $B_x$  field computed from the velocity fields is replaced by the accurate value  $B_{xm}$  deduced from the simulation output  $\theta_{c1}$  field. The retrieved temperature field is much more similar to the original  $\theta_{c1}$  field (compare Figs. 3f, 5a and 6c, and compare the difference fields in Figs. 5b and 6d). The cold pool is still weak and less broad since it is influenced by the  $B_r$  deduced from the thermodynamic equation in connection with the underestimation of evaporation of raindrops. The warm air extending upward and rearward from the gust front is nearly perfectly retrieved. There is only one maximum axis at 6.5 km (instead of two in Fig. 5a), as should be the case. In contrast, another retrieval experiment, which keeps the  $B_x$  but replaces  $B_r$  with  $B_{rm}$  deduced from the model  $\theta_{c1}$  field, gives the retrieved temperature field with virtually no improvement (not shown here). These results show that the main errors in retrievals performed on the time-averaged fields are associated with neglecting the eddy flux terms in (5). This conclusion is consistent with the difference fields in Figs. 5b and 6d, as the local maximum error falls in the region of the warm tongue. That feature is associated with convective cells, which are the primary agents responsible for the fluctuating fields giving rise to the eddy terms. The generally fa-

vorable comparison between the model and retrieved fields in Figs. 3f and 5a throughout the stratiform region (as evident in the difference field in Fig. 5b) suggests that retrievals applied to mean or composite radar data fields will be more accurate in the stratiform region than in the highly convective region of the leading line, where the eddy fluxes are probably strong.

Since the eddy flux terms involve perturbations and correlations of the velocity components, it is evident that they are related to convective-scale momentum fluxes. If these fluxes could be parameterized, the retrieval technique could be improved so that it could be applied in the convective region with more confidence. However, the parameterization of momentum fluxes is a difficult problem, and it is not immediately obvious how they could be parameterized in the context of the retrieval.

### 5. Application of the retrieval to the model instantaneous fields

We have now seen that reasonably accurate results may be expected if the retrieval is applied to the time-mean wind fields of the stratiform region of a squall line with a trailing stratiform region; however, the highly fluctuating wind fields in the convective region lead to errors in the retrieval applied to the mean winds in that zone. In the absence of some parameterization of the missing eddy flux terms, it is necessary to apply the retrieval to the instantaneous wind field in the convective region in order to infer the thermodynamic structure of the convective zone. In this section, we explore the accuracy of the retrieval when it is applied

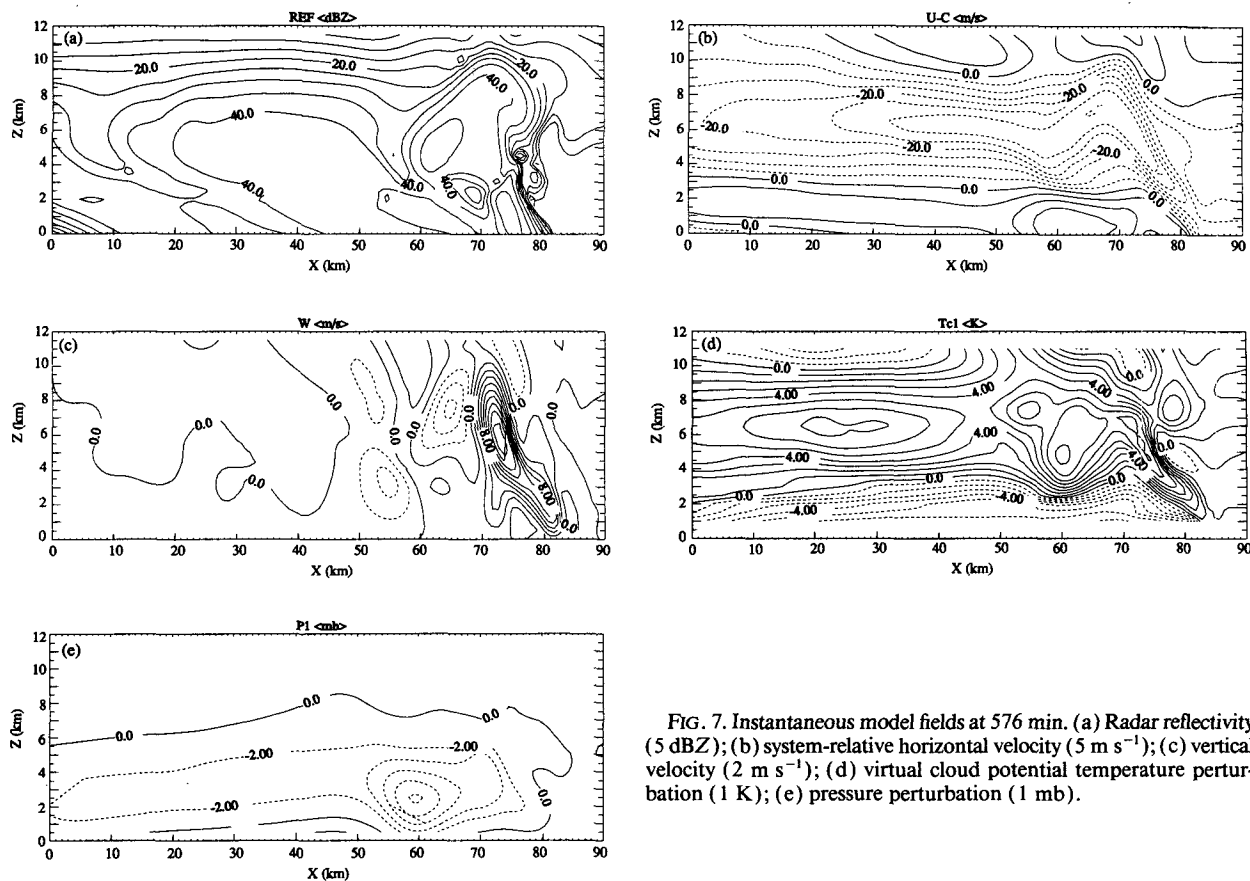


FIG. 7. Instantaneous model fields at 576 min. (a) Radar reflectivity (5 dBZ); (b) system-relative horizontal velocity ( $5 \text{ m s}^{-1}$ ); (c) vertical velocity ( $2 \text{ m s}^{-1}$ ); (d) virtual cloud potential temperature perturbation (1 K); (e) pressure perturbation (1 mb).

to the instantaneous fields. In particular, the time resolution required to obtain accurate results is investigated, the third objective mentioned in the introduction. The time resolution is important to establish because it implies how close together in time individual radar scans must be obtained to assure the accuracy of the retrieval.

#### a. Retrieval at 576 min

The instantaneous model fields at 576 min are for a time slightly before the main cell reached its maximum rainfall intensity, which was increasing sharply (Fig. 2b). It is expected that at such a time the non-linearity of the evolution may be less important than at a ridge or trough. The reflectivity field (Fig. 7a) clearly distinguishes the convective region in the front from the stratiform region behind. They are separated by a weak-reflectivity zone centered at  $X = 56 \text{ km}$ . The horizontal system-relative airflow has a pattern similar to that of the time-averaged flow, except that the axis of maximum front-to-rear flow describes an upward arc shape in the convective region, that is, stronger variability in the cross-line direction (Fig. 7b). The vertical velocity field (Fig. 7c) appears quite different

from that of the time-averaged case. The intensities are much greater (maximum updraft is  $19 \text{ vs } 11 \text{ m s}^{-1}$ ; maximum downdraft is  $-6 \text{ vs } -1.2 \text{ m s}^{-1}$ ). The alternating updrafts and downdrafts demonstrate more cellular structure, which was strongly filtered in the time-averaging process applied in section 4. Several local maxima are found corresponding to these drafts in the  $\theta_{c1}$  field (Fig. 7d). The warm tongue extending upward from the gust front coincides with the main updraft and indicates how the warm air at upper levels originates from lower levels. The horizontally oriented

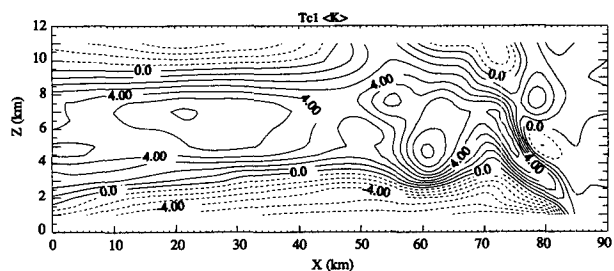


FIG. 8. Virtual cloud potential temperature perturbation retrieved from  $B_{xm}$  and  $B_{im}$  deduced from the model-output  $\theta_{c1}$  field at 576 min.

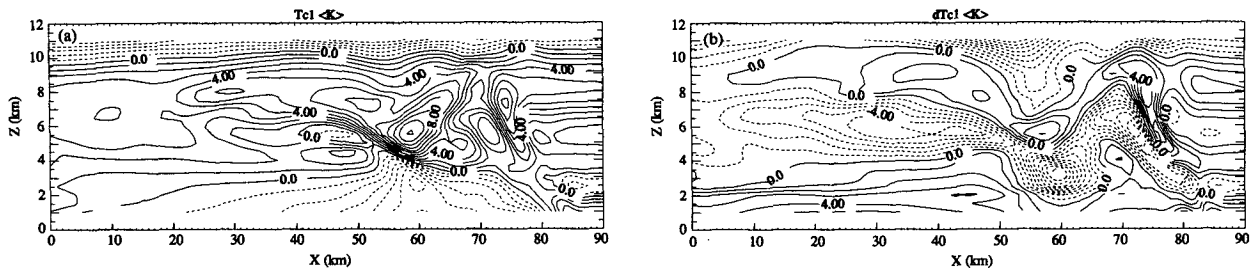


FIG. 9. (a) Retrieved  $\theta_{c1}$  field without taking into account of local time derivatives; (b) difference field of (a).

maximum in the rear half of the domain is associated with the mesoscale updraft of the stratiform region. The maxima seen at altitudes 4–8 km between  $X = 50$  and 70 km in Fig. 7d seem to be correlated with the downdrafts in Fig. 7c. This finding suggests that the downdrafts at these locations between the main convective line and the stratiform region are driven by dynamic forcing rather than by negative buoyancy. The complexity of the  $\theta_{c1}$  field presents a stringent challenge to the retrieval technique.

As in the last section, a verification of the computational method is made first; that is, with  $B_{xm}$  and  $B_{tm}$ , deduced directly from the model output  $\theta_{c1}$  field; then the  $\theta_{c1}$  field is retrieved, which fits  $B_{xm}$  and  $B_{tm}$  simultaneously in the least-squares sense. The constants involved in (8) are again set to get the best result,<sup>2</sup> which is shown in Fig. 8. The retrieved  $\theta_{c1}$  field has nearly all the details that appeared in the model output (Fig. 7) except for the underestimation of positive perturbations at upper levels (by about 1°C). It is evident that the retrieved temperature should be valid unless the  $B_x$  and  $B_t$  are incorrectly deduced from the equation of motion and the thermodynamic equation. Thus, we conclude again that the basic computational technique is valid.

In order to measure the total impact of the local change of wind field on the retrieval, the calculations were next made from  $B_x$  and  $B_t$  but without local time derivatives. Although there are positive perturbations at upper levels and negative ones below, the original  $\theta_{c1}$  field is not distinguishable (Fig. 9a). Its difference field (Fig. 9b) shows peak errors of  $-4^\circ$  to  $-8^\circ\text{C}$ , indicating that the evolution of the simulated squall line is much too important to be neglected. Since the simulated squall line does not always evolve linearly, the estimated values of local time derivatives change when the interval centered at a particular time varies. The question is: How close together in time must the observations be to obtain a sufficiently accurate  $B_x$  and

$B_t$  for the retrieval? Table 1 indicates the accumulated errors  $E_{B_x}$  and  $E_{B_t}$ , defined as

$$E_{B_x} = \frac{\iint (B_x - B_{xm})^2 dx dz}{\iint (B_{xm})^2 dx dz},$$

$$E_{B_t} = \frac{\iint (B_t - B_{tm})^2 dx dz}{\iint (B_{tm})^2 dx dz},$$

when  $B_x$  and  $B_t$  are calculated with different intervals.<sup>3</sup> When the local time derivatives are taken into account, both  $B_x$  and  $B_t$  are greatly improved. However, the error for calculations centered at 576 min is not very sensitive to the size of the time interval since the tendency around this time is quite linear. For purposes of illustration, the  $\pm 1$ -min interval has been chosen. The moist adiabat of 21°C was used. The retrieval results and related difference fields are shown in Fig. 10. The retrieved temperature perturbations (Fig. 10a) demonstrate a great improvement with respect to those in Fig. 9, where no information about the temporal changes was provided. The differences between model and retrieved values are greatly reduced, although errors of  $\sim 2^\circ\text{C}$  in magnitude remain (compare Figs. 9b and 10b). Most of the features that appear in the model output  $\theta_{c1}$  field (Fig. 7d) are now qualitatively apparent. The cold pool at lower levels is similar although the nose shape seems to be exaggerated. The warm tongue rising up from the gust front over the cold pool is evident, though still a little weak. The two other local maxima just behind the warm tongue and that in the stratiform region with a horizontal orientation are also retrieved. The cold air at upper levels in the rear part of domain and the couplet of cold and warm cores over the warm tongue are recognizable although they are not especially well defined. The retrieval of pressure

<sup>2</sup> The constants  $V_0$ ,  $\mu_0$ , and  $\mu_1$  are not universal; they are related to fields to be retrieved and corresponding wind fields and have to be tuned based on experience.

<sup>3</sup> The interval of  $\pm 2$  min represents a time interval of 4 min.

TABLE 1. Deviations of  $B_x$  and  $B_{tm}$  at 576 min with and without taking into account the local time derivatives.

Time interval	$E_{B_x}$	$E_{B_t}$
No	2.49	1.22
$\pm 2$ min	0.76	0.52
$\pm 1$ min	0.55	0.48
$\pm 15$ s	0.50	0.52

perturbation (Fig. 10c) is also successful. The overall shape of contours is very close to the model output (Fig. 7e). The results for the other time intervals indicated in Table 1 (not shown) are nearly as good as those in Fig. 10.

The retrieval at 576 min with the local time derivatives taken into account thus gives us some encouragement. However, these results are somewhat deceptive because of the rather linear evolution occurring at 576 min. To get a more complete view of the impact of the temporal evolution, the retrieval is now carried at another moment in the storm's lifetime.

#### b. Retrieval at 566 min

In contrast to 576 min, the surface rainfall at 566 min has just passed through a secondary maximum, and the tendency is strongly decreasing (Fig. 2b). Hence, it is suspected that the time changes are not linear and may not be well captured by a centered time difference (as would be computed from two successive radar scans). The reflectivity field (Fig. 11a) also shows

different characteristics at the front edge of the storm with respect to that seen at 576 min (Fig. 7a). The new cell has not yet reached its full development as demonstrated by the lower upward extension of the 40-dBZ contour. There are two front-to-rear airflow tongues, above  $X = 80$  and  $X = 68$  km (Fig. 11b), which correspond to the newly developing cell and the decaying cell (Fig. 11c). Although the maximum vertical velocity is at a lower altitude ( $Z = 4$  km), its magnitude is  $19 \text{ m s}^{-1}$ , the same intensity as at 576 min. This structure is characteristic of a growing cell. The positive potential temperature perturbation at  $X = 68$  km (Fig. 11d) is associated with the main convective updrafts (Fig. 11c). The pair of local maximum and minimum  $\theta_{c1}$  at altitudes of 5 and 8 km at  $X = 71$  km in Fig. 11d coincide with convective downdraft motion seen in Fig. 11c. The opposite signs of these two perturbations indicate that the very deep downdraft between the two updrafts was formed through more than one mechanism. The upper portion ( $Z > 7.5$  km) is positively buoyant and evidently driven by dynamic forcing such as upper-level convergence. The middle portion ( $3 < Z < 7.5$  km) corresponds to the cool-air pocket, behind the major warm core, which originates from the midlevel low- $\theta_e$  environmental air ahead of the storm. The lower portion ( $Z < 3$  km) is driven by the negative buoyancy produced by evaporation of rainwater falling from the major cell. These downdraft mechanisms are the subject of a future paper (Sun et al. 1992).

A verification of the computational step was again carried out with  $B_{xm}$  and  $B_{tm}$  deduced from the model-output  $\theta_{c1}$  field. The result (Fig. 12) assures again that

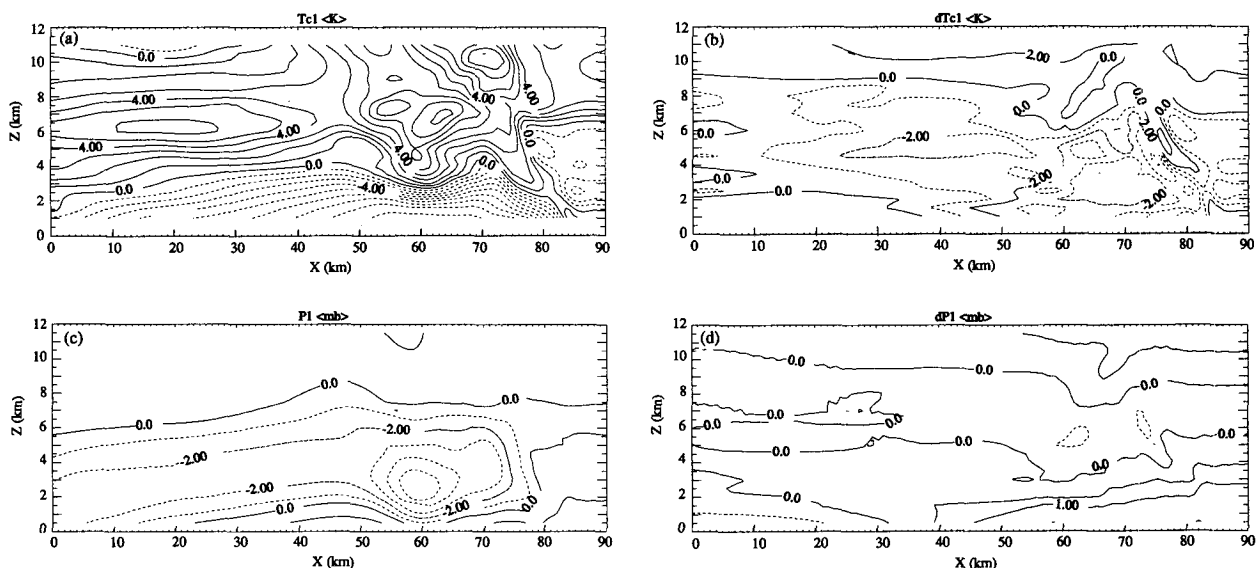


FIG. 10. (a) Retrieved  $\theta_{c1}$  field with local time derivatives calculated from  $\pm 1$ -min interval; (b) difference field of (a); (c) retrieved  $p_1$  field; (d) difference field of (c).

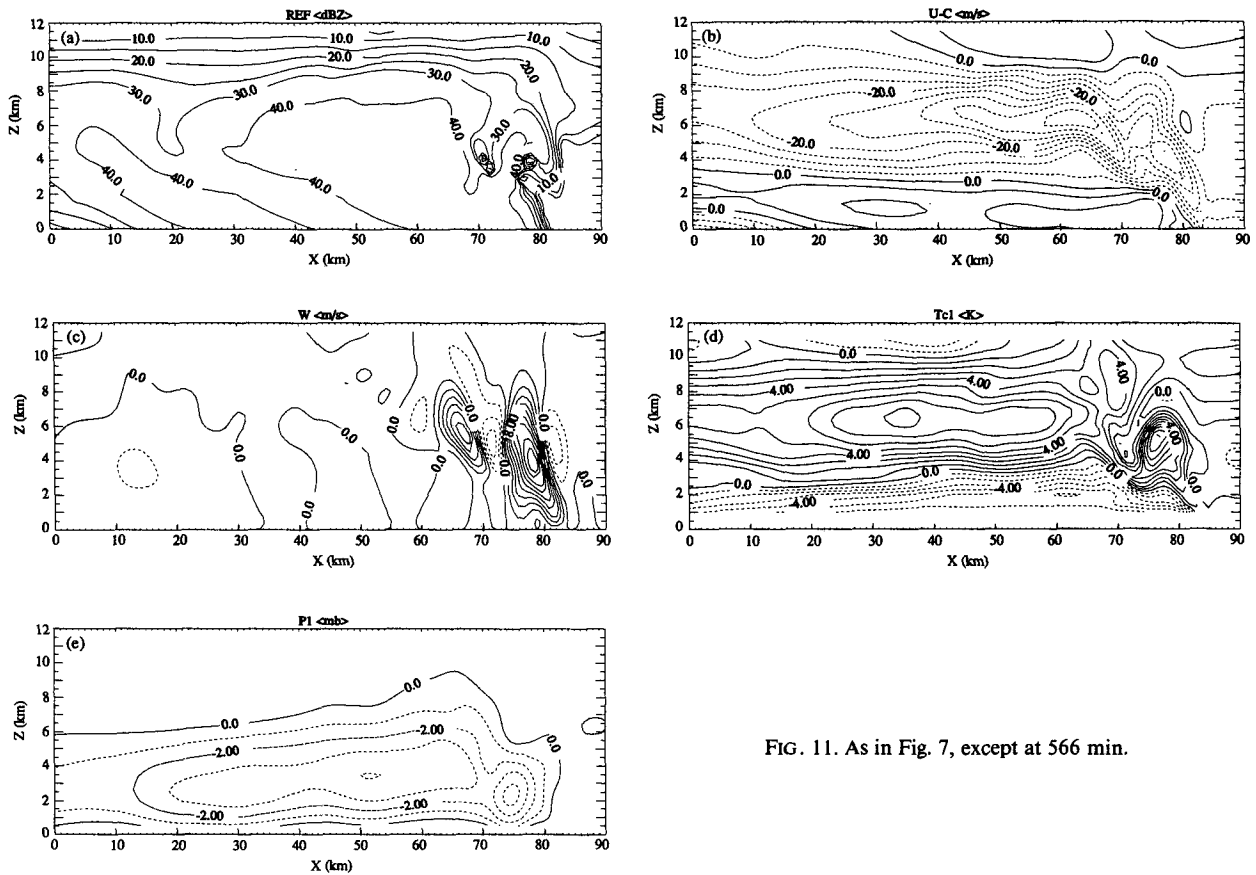


FIG. 11. As in Fig. 7, except at 566 min.

there is no major problem related to the computational technique, except the slight weakness of positive perturbations ( $\sim 1^\circ\text{C}$ ). The retrieval without the local time derivatives (not shown here) again gives us a virtually meaningless result. Table 2 demonstrates clearly the deviation of  $B_x$  and  $B_t$  from  $B_{xm}$  and  $B_{tm}$  when different intervals centered at 566 min are used. The moist adiabat is again  $21^\circ\text{C}$ . The estimation of  $B_x$  and  $B_t$  is greatly improved when local time derivatives calculated over smaller time intervals are included, particularly for  $B_x$ , whose deviation is 7.8 at 566 min versus 2.5 at 576 min without taking into account local

time derivatives. The inclusion of local time derivatives improves the estimation of  $B_x$ ; however,  $B_x$  at 566 min with a  $\pm 15$ -s interval is still high: 1.3 versus 0.5 at 576 min. This reflects that the temporal changes around 566 min are more important and less linear than at 576 min.

When the interval is fixed at  $\pm 15$  s, we find that  $B_t$  could be improved if the moist adiabat of wet-bulb potential temperature  $16^\circ\text{C}$  is used instead of  $21^\circ\text{C}$ . Although a similar result was found at 576 min (the best estimation of  $B_t$  is given by the moist adiabat of  $18^\circ\text{C}$ ), little impact on the retrieved temperature perturbations was evident. This is not true at 566 min. The retrieval with the moist adiabat of  $16^\circ\text{C}$  gives the temperature perturbations (Fig. 13a) clearly better than

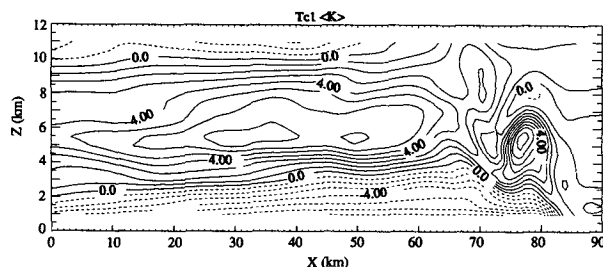


FIG. 12. As in Fig. 8, except at 566 min.

TABLE 2. As in Table 1, except at 566 min.

Time interval	$E_{B_x}$	$E_{B_t}$
No	7.80	1.38
$\pm 2$ min	4.24	0.62
$\pm 1$ min	2.18	0.44
$\pm 15$ s	1.33	0.41

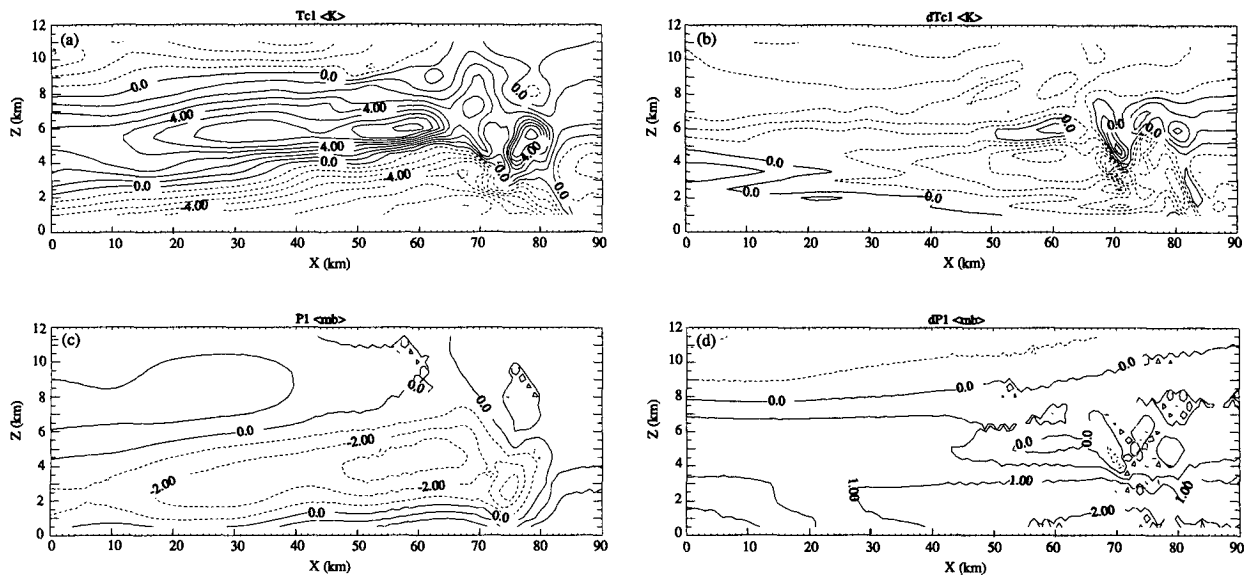


FIG. 13. (a) Retrieved  $\theta_{c1}$  field with local time derivatives calculated from  $\pm 15$ -s interval; (b) difference field of (a); (c) retrieved  $p_1$  field; (d) difference field of (c).

21°C (not shown here). Compared with the model-output  $\theta_{c1}$  field (Fig. 11d), the main features are observed: the cold pool below (although it extends too far upward between  $X = 60$  and  $X = 70$  km), the warm-air area above with the local maximum extending upward from the gust front, the horizontal axis of maximum at the 6-km level (500 m lower than the model output), and the cold air at upper levels. At time intervals of  $\pm 1$  and  $\pm 2$  min (Figs. 14a,b), most of the features evident in the model simulation are still present, in a qualitative sense, but are grossly exaggerated quantitatively. This impression is consistent with Table 2 and suggests that in a situation of highly nonlinear evolution, the convective-region thermodynamics will be impossible to retrieve with typical scan intervals of present-day Doppler weather radars. Since it is difficult to know from radar data whether or not the changes in the convective region are linear, great caution should be exercised in applying retrieval techniques to the convective region. This result emphasizes the importance of developing rapid-scan radar technology for use in meteorology.<sup>4</sup> This result also emphasizes the danger of blindly performing retrieval analysis; the results may look reasonable qualitatively but be in large error quantitatively.

Figure 13 shows the better result obtained with a moist adiabat 5°C less than that of the mean lower-level environmental air (21°C). The better result ob-

tained at the lower value of wet-bulb potential temperature may just be fortuitous. However, it more likely reflects the fact that turbulent mixing of low- $\theta_w$  air into the updraft (Zipser 1977) lowered the amount of condensation in the updraft core. The mixing parameterization is not explicitly included in the model; however, the finite-difference procedure involved both in the simulation and in the retrieval plays a similar role (R. G. Fovell, personal communication). The turbulent-mixing effect seems less important at 576 min. At that time, the rainfall was almost at its peak intensity, and the main updraft core was more vigorous. Thus, the mixing should have been relatively weak at that time.

## 6. Conclusions

The work described above accomplishes the validation of the retrieval technique previously applied by RS to a West African squall line by applying it to the output fields of a numerical model simulation of a similar squall line. To focus the validation study and make it a useful guide for future work, we set the three objectives listed in the Introduction.

The first objective was simply to determine if the computational methods of the retrieval are accurate. They were found to be valid when applied both to model time-averaged fields and to instantaneous fields.

The second objective was to determine whether the mean thermodynamic structure of the storm could be determined from the time-mean winds of the model simulation. This determination is important since the Doppler radar scans a volume much smaller than the

<sup>4</sup> The need for rapid-scan radar for improving resolution in Doppler radar studies of convection has been discussed by Carbone et al. [1980 (see pp. 1176, 1177, 1182, 1186, and 1194), 1985].

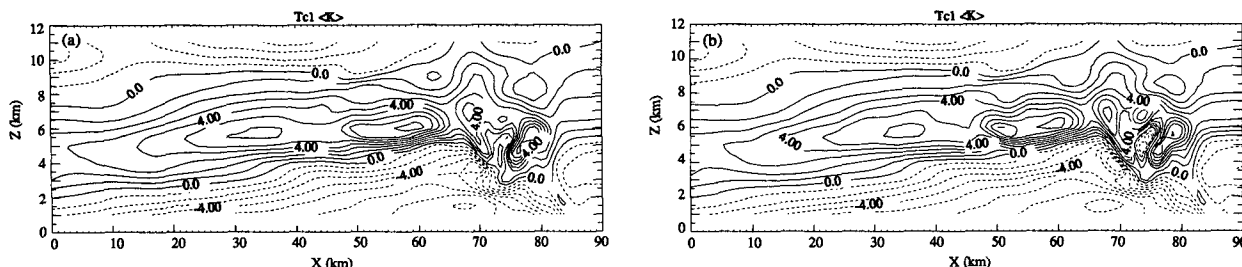


FIG. 14. (a) As in Fig. 13a, but with  $\pm 1$ -min interval; (b) as in Fig. 13a, but with  $\pm 2$ -min interval.

total storm, and one method of analysis is to combine data from several scans into a composite analysis, which represents a kind of mean storm structure. This procedure has been followed in the analysis of West African squall lines (Sun and Roux 1988; RS) and in work on the 10–11 June PRE-STORM squall line (Biggerstaff and Houze 1991a,b). The results obtained here, by applying the retrieval to time-mean model-output fields, indicate that the retrieval reproduces the thermodynamic structure of the stratiform region from the mean wind fields reasonably accurately. However, eddy correlations of the temporally fluctuating wind fields in the convective region, which are not included in the retrieval calculations, can lead to significant errors in results for the convective regions.

Since one cannot obtain sufficiently accurate results in the convective region of the squall line with a trailing stratiform region from the mean wind fields alone, it becomes necessary to perform retrievals for instantaneous wind fields. This fact led to the question posed by our third objective: What time resolution is required to obtain reliable results from the retrieval when applying the technique to instantaneous fields in the highly fluctuating convective region? Experiments applying the retrieval to the model simulation for two different times show that when the time changes are large and nonlinear, very high time resolution is required. Unambiguous results in these situations cannot be obtained if the spacing between wind observations exceeds about 2 min. This result implies that very high scan rates would be required to assure accurate results for all situations. Longer intervals (e.g., 4 min) may be suitable if the time changes are linear. Since it is difficult to recognize in real data (especially in real time) whether the time changes in the convection are linear or not, this result implies a major limitation on the applicability of retrievals to convective regions. There is a danger of applying retrieval to situations in which the time changes are nonlinear. Retrievals may look qualitatively reasonable but be drastically in error quantitatively. This result further suggests that the development of rapid-scan radar technology will greatly aid the study of convective storms by making it possible for thermodynamical retrievals to be more reliable.

In addition to the above problems we have found that the underestimation of precipitation content  $q_r$  results in the underestimation of vertical gradients of retrieved temperature perturbation fields, that is, underestimation of both positive perturbations at upper levels and negative perturbations at lower levels, and that the retrieval is sensitive to the choice of the moist adiabat used in the thermodynamic calculations. This sensitivity is probably related to turbulent mixing and merits caution when applying the retrieval.

*Acknowledgments.* The main software used in this study was developed originally by Dr. Frank Roux at Centre de Recherches en Physiques de l'Environnement Terrestre et Planetaire (CRPE/CNET-CNRS) in Issy-Les-Moulineaux, France. Model output was very kindly provided for this study by Dr. Robert Fovell. Dr. Dean Churchill provided valuable advice and G. C. Gudmundson edited the manuscript. This research was sponsored by National Science Foundation Grant ATM-8719838.

#### REFERENCES

- Biggerstaff, M. I., and R. A. Houze Jr., 1991a: Kinematic and precipitation structure of the 10–11 June 1985 squall line. *Mon. Wea. Rev.*, **119**, 3034–3065.
- , and —, 1991b: Midlevel vorticity structure of the 10–11 June 1985 squall line. *Mon. Wea. Rev.*, **119**, 3066–3079.
- Byers, H. R., and R. R. Braham, 1949: *The Thunderstorm*. U.S. Government Printing Office, 287 pp.
- Carbone, R. E., M. J. Carpenter, and C. D. Burghart, 1985: Doppler-radar sampling limitations in convective storms. *J. Atmos. Ocean. Technol.*, **2**, 357–361.
- , F. I. Harris, P. H. Hildebrand, R. A. Kropfli, L. J. Miller, W. Moniger, R. G. Strauch, R. J. Doviak, K. W. Johnson, S. P. Nelson, P. S. Ray, and M. Gilet, 1980: The Multiple Doppler Radar Workshop, November 1979. *Bull. Amer. Meteor. Soc.*, **61**, 1169–1203.
- Charba, J., 1974: Application of the gravity current model to analysis of squall-line gust fronts. *Mon. Wea. Rev.*, **102**, 140–156.
- Droegemeier, K. K., and R. B. Wilhelmson, 1987: Numerical simulation of thunderstorm outflow dynamics. Part I: Outflow sensitivity experiments and turbulence dynamics. *J. Atmos. Sci.*, **44**, 1180–1210.
- Fovell, R. G., and Y. Ogura, 1988: Numerical simulation of a mid-latitude squall line in two dimensions. *J. Atmos. Sci.*, **45**, 3846–3879.
- Gal-Chen, T., 1978: A method for the initialization of the anelastic

- equation: Implication for matching models with the observations. *Mon. Wea. Rev.*, **106**, 587–606.
- Hane, C. E., and B. C. Scott, 1978: Temperature and pressure perturbations within convective clouds derived from detailed air motions: Preliminary testings. *Mon. Wea. Rev.*, **106**, 651–661.
- , R. B. Wilhelmson, and T. Gal-Chen, 1981: Retrieval of thermodynamic variables within deep convective clouds: Experiments in three dimensions. *Mon. Wea. Rev.*, **109**, 564–576.
- Houze, R. A. Jr., B. F. Smull, and P. Dodge, 1990: Mesoscale organization of springtime rainstorms in Oklahoma. *Mon. Wea. Rev.*, **117**, 613–654.
- , S. A. Rutledge, M. I. Biggerstaff, and B. F. Smull, 1989: Interpretation of Doppler weather-radar displays of midlatitude mesoscale convective systems. *Bull. Amer. Meteor. Soc.*, **70**, 608–619.
- Klemp, J. B., and R. B. Wilhelmson, 1978: Simulations of right- and left-moving storms produced through storm-splitting. *J. Atmos. Sci.*, **35**, 1097–1110.
- Ogura, Y., and M.-T. Liou, 1980: The structure of a midlatitude squall line. *J. Atmos. Sci.*, **37**, 553–567.
- Roux, F., 1985: Retrieval of thermodynamic fields from multi-Doppler radar data using the equations of motion and the thermodynamic equation. *Mon. Wea. Rev.*, **113**, 2142–2157.
- , 1988: The West African squall line observed on 23 June 1981 during COPT81: Kinematics and thermodynamics of the convective region. *J. Atmos. Sci.*, **45**, 406–426.
- , and J. Sun, 1990: Single-Doppler observations of a West African squall line on 27–28 May 1981 during COPT 81: Kinematics, thermodynamics and water budget. *Mon. Wea. Rev.*, **118**, 1826–1854.
- , J. Testud, M. Payen, and B. Pinty, 1984: West African squall-line thermodynamic structure retrieved from dual-Doppler radar observations. *J. Atmos. Sci.*, **41**, 3104–3121.
- Smull, B. F., and R. A. Houze Jr., 1985: A midlatitude squall line with a trailing region of stratiform rain: Radar and satellite observations. *Mon. Wea. Rev.*, **113**, 117–133.
- , and —, 1987: Dual-Doppler radar analysis of a midlatitude squall line with a trailing region of stratiform rain. *J. Atmos. Sci.*, **44**, 2128–2148.
- Soong, S. T., and Y. Ogura, 1980: Response of tradewind cumuli to large-scale processes. *J. Atmos. Sci.*, **37**, 2035–2050.
- Sun, J., and F. Roux, 1988: Thermodynamic structure of the trailing stratiform regions of two West African squall lines. *Ann. Geophys.*, **6**, 659–670.
- , R. A. Houze Jr., R. G. Fovell, and M. I. Biggerstaff, 1992: Thermodynamic structure of the trailing stratiform region of a squall line. Submitted.
- Wakimoto, R. M., 1982: The life cycle of thunderstorm gust fronts as viewed with Doppler radar and rawinsonde data. *Mon. Wea. Rev.*, **110**, 1060–1082.
- Wilhelmson, R. E., and Y. Ogura, 1972: The pressure perturbation and the numerical modeling of a cloud. *J. Atmos. Sci.*, **29**, 1295–1307.
- Zipser, E. J., 1977: Mesoscale and convective-scale downdrafts as distinct components of squall-line circulation. *Mon. Wea. Rev.*, **105**, 1568–1589.